IUST
Iran University of Science and Technology

Iranian Journal of Electrical and Electronic Engineering

Journal Homepage: ijeee.iust.ac.ir

Research Paper

The Effect of Dummy Slots on Machine Performance in Brushless Permanent Magnet Machines: An Analytical, Numerical, and Experimental Study

A. Jabbari*(C.A.)

Abstract: Low-speed brushless permanent magnet machines are ideal for use in gearless propulsion systems. It is important to provide a precise analytical model to determine the performance characteristics of these machines. One of the challenges in designing permanent magnet machines is the elimination of the pulsating torque due to the presence of cogging torque and torque ripple components. The use of dummy slots (auxiliary teeth) is one of the most common methods of reducing pulsating torque phenomenon. In this paper, an accurate two-dimensional analytical model for calculating the magnetic vector potential in brushless permanent magnet machines is presented, taking into account the effect of stator slots, stator dummy slots, the magnetic direction of permanent magnets and phase winding style. The proposed analytical method is based on solving Laplace's and Poisson's equations using the separation of variables method for given regions in the subdomain approach. In the proposed method, to achieve a simpler analytical model, by changing the variable, the polar coordinate system is converted to a quasi-Cartesian coordinate system. Therefore, in mathematical terms, the hyperbolic functions are used instead of exponential ones. To validate the proposed model accuracy, the performance of a 14 kW low-speed brushless permanent magnet motor is calculated analytically and compared with the results of the numerical method and the experimental tests. Comparison of the performance results of this motor shows the consistency of analytical, numerical, and experimental results.

Keywords: Analytical Modeling, Brushless Permanent Magnet Machine, Dummy Slots, Experimental Tests, FEA, Subdomain Method.

1 Introduction

LOW-SPEED brushless permanent magnet machines are notable for their high power, high efficiency, and high reliability for use in gearless propulsion systems and wind turbine applications. By using these machines, the gearbox can be removed from the system, and in addition to reducing noise and improving the maintenance period, system losses can be significantly reduced. However, the noise and vibrations caused by the pulsating torque phenomenon greatly affect the performance of the machine. One of the components of pulsation torque is the cogging torque caused by the interaction of the rotor's permanent magnets and the stator's slotted core. Various methods have been proposed to reduce cogging torque in permanent magnet machines. The technique of skewing of the stator teeth [1-4], selecting the appropriate ratio of the pole width to pole pitch or the slot width to slot pitch [5], and using dummy slots [6-8] are the most common methods used to reduce cogging torque. When using the dummy slot method, it is very important to determine the exact number and dimensions of the slots. Therefore, accurate estimation of the magnetic vector potential for calculating machine performance such as cogging torque, electromagnetic torque, back electromotive

Iranian Journal of Electrical and Electronic Engineering, 2022.
Paper first received 14 September 2021, revised 11 December 2021, and accepted 17 December 2021.
* The author is with the Department of Mechanical Engineering, Arak University, Arak, Iran.
E-mail: a-jabbari@araku.ac.ir.
Corresponding Author: A. Jabbari.
https://doi.org/10.22068/IJEEE.18.2.2284

force, self-inductance, and mutual inductance, as well as determining the optimal values of design parameters is essential.

Various methods, including analytical and numerical methods, have been used to calculate the distribution of magnetic flux density in electric machines. While accurate results can be obtained by using numerical methods such as finite element analysis, the use of these methods, especially in the first stage of the design process, will be very time-consuming. Analytical methods such as conformal mapping [9-12], magnetic equivalent circuit [13-15], subdomain model [16-23], and calculation of relative permeability of slots [24, 25] have been reported that for modeling electric machines in the initial design stage and design optimizations are useful. The subdomain model has higher accuracy than other analytical methods. This method is based on the resolution of Laplace's and Poisson's equations in different regions by applying the appropriate boundary conditions in the electric machine.

According to studies, there are few analytical models for calculating the magnetic field in brushless permanent magnet machines [9, 18, 20, 24, 25]. No reference in the literature was found to the provision of a precise analytical model for calculating the magnetic velocity potential in brushless permanent magnet machines with stator dummy slots. Also, in most of the presented articles, the validation of the results has been done by numerical method. Also, in the analytical models presented by the subdomain method for radial flux machines, hyperbolic functions have not been used so far.

This paper presents a detailed analytical model for calculating the magnetic vector potential in a brushless permanent magnet machine. The proposed analytical method is based on the equations of Laplace, Poisson, and Maxwell in pseudo-Cartesian coordinates and applies boundary conditions and proper interface conditions. In the developed model, the effect of the stator dummy slots has been considered and for ease of modeling, hyperbolic functions have been used instead of exponential functions by applying the variable change and converting the polar coordinates system to the pseudo-Cartesian coordinate system. It has been shown that using the proposed model, it is possible to estimate the performance characteristics of a brushless permanent magnet machine such as air gap flux density, cogging torque, electromagnetic torque, back electromotive force, self-inductance, and mutual inductance. The proposed model is used to calculate the performance of a prototype 14 kW-150 rpm brushless permanent magnet motor, in which the dummy slot method is used to reduce the motor pulsating torque components. To validate the analytical model, by performing two-dimensional numerical modeling in the Maxwell software environment and fabrication of a prototype motor, the analytical, numerical, and experimental results were compared. It has been shown that analytical results are in good agreement with the results of numerical and experimental studies.

The definition of the problem and the assumptions are stated in Section 2. Analytical expressions of the magnetic vector potential in each subdomain are formulated in Section 3. The calculation of performance and model validation is described in Section 4.

2 Problem and Coordinates System Definition

In this section, we first introduce the brushless permanent magnet motor, the parameters of the motor, and the division of the motor into different regions. Then, how to convert the polar coordinate system to the pseudo-Cartesian coordinates system is explained.

2.1 Introduction of the BLDC Motor Parameters

The two-dimensional view of a three-phase surface-mounted magnet BLDC machine with an internal rotor and a slotted core and a two-layer winding is shown in Fig. 1. The parameters of the machine and the model regions are defined in Fig. 2 in the R–θ polar coordinates system. The machine model is divided into five subdomains. The stator has three subdomains including $Q1$ slots area (j region), $Q1$ open slots area (i region), and $Q2$ dummy slots area (k region). The rotor has a permanent magnet region (region I). The air-gap area (region II) is the distance between the outer surface of the rotor and the inner surface of the stator. The angular position of i-th stator slot, i-th stator open slot, i-th dummy slot are expressed in Eqs. (1) to (3), respectively.

$$\theta_j = -\frac{\alpha}{2} + \frac{2i\pi}{Q_1} \qquad 1 \le i \le Q_1 \tag{1}$$

$$\theta_i = -\frac{\beta}{2} + \frac{2i\pi}{Q_1} \qquad 1 \le i \le Q_1 \tag{2}$$

$$\theta_k = -\frac{\gamma}{2} + \frac{2i\pi}{Q_2} \qquad 1 \le i \le Q_2 \tag{3}$$

2.2 A Pseudo-Cartesian Coordinates System Definition

The Laplace equation can be expressed in the polar coordinates system as follows:

$$\frac{\partial^2 A}{\partial r^2} + \frac{1}{r}\frac{\partial A}{\partial r} + \frac{1}{r^2}\frac{\partial^2 A}{\partial \theta^2} = 0 \quad \text{for} \quad \begin{cases} R_1 \le r \le R_2 \\ \theta_1 \le \theta \le \theta_2 \end{cases} \tag{4}$$

By replacing the variable $r = R_1 e^{-t}$, Eq. (4) in the polar coordinate system converts to (5) in the pseudo-Cartesian coordinate system.

$$\frac{\partial^2 A}{\partial t^2} + \frac{\partial^2 A}{\partial \theta^2} = 0 \quad \text{for} \quad \begin{cases} \ln\left(\frac{R_1}{R_2}\right) \le t \le 0 \\ \theta_1 \le \theta \le \theta_2 \end{cases} \tag{5}$$

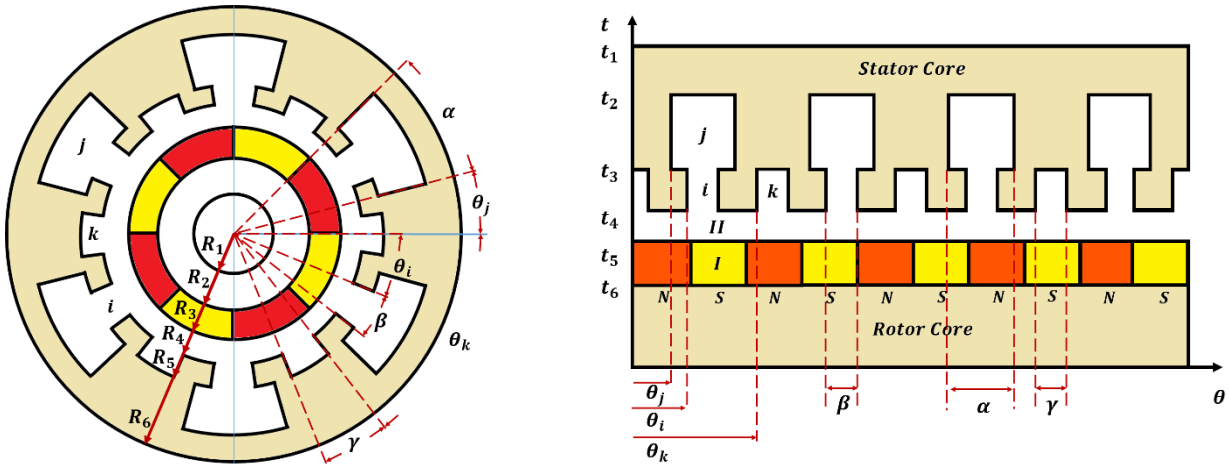

(a) (b)

Fig. 1 Definition of the BLDC machine subdomains in the a) *R*–*θ* coordinates system and b) *t*–*θ* coordinates system.

Table 1 PDE equations related to each subdomain.

PDEs equations		Region Ω	Domain
$\frac{\partial^2 A_\Omega}{\partial t^2}+\frac{\partial^2 A_\Omega}{\partial \theta^2}=0$	(Laplace's Equation)	*i*	$\begin{cases} t_3=\ln(R_3/R_4)\le t\le t_4=0 \\ \theta_i\le\theta\le\theta_i+\beta \end{cases}$
		k	$\begin{cases} t_3=\ln(R_3/R_4)\le t\le t_4=0 \\ \theta_k\le\theta\le\theta_k+\gamma \end{cases}$
		II	$\begin{cases} t_5=\ln(R_2/R_3)\le t\le t_6=0 \\ 0\le\theta\le 2\pi \end{cases}$
$\frac{\partial^2 A_\Omega}{\partial t^2}+\frac{\partial^2 A_\Omega}{\partial \theta^2}=-\mu_0 J$	(Poisson's Equation)	*j*	$\begin{cases} t_1=\ln(R_4/R_5)\le t\le t_2=0 \\ \theta_j\le\theta\le\theta_j+\alpha \end{cases}$
$\frac{\partial^2 A_\Omega}{\partial t^2}+\frac{\partial^2 A_\Omega}{\partial \theta^2}=-\frac{\mu_0}{r}\left(M_\theta-\frac{\partial M_r}{\partial\theta}\right)$		*I*	$\begin{cases} t_7=\ln(R_1/R_2)\le t\le t_8=0 \\ 0\le\theta\le 2\pi \end{cases}$
for radial magnetization $\begin{cases} M_{rn}=\frac{4B_r}{\mu_0 n\pi}\sin\left(\frac{n\pi\alpha_p}{2}\right) \\ M_{\theta n}=0 \end{cases}$			
for parallel magnetization $\begin{cases} M_{rn}=\frac{B_r}{\mu_0}\alpha_p.\left[A_{1n}(\alpha_p)+A_{2n}(\alpha_p)\right] \\ M_{\theta n}=\frac{B_r}{\mu_0}\alpha_p.\left[A_{1n}(\alpha_p)-A_{2n}(\alpha_p)\right] \end{cases}$		$A_{1n}(\alpha_p)=\sin\left((np+1)\frac{\pi\alpha_p}{2p}\right)/(np+1)\frac{\pi\alpha_p}{2p}$ $A_{2n}(\alpha_p)=\begin{cases}\sin\left((np-1)\frac{\pi\alpha_p}{2p}\right)/(np-1)\frac{\pi\alpha_p}{2p} & \text{for } np\neq 1 \\ 1 & \text{for } np=1\end{cases}$	

Fig. 1(b) shows the different areas of the BLDC permanent magnet machine in the pseudo-Cartesian coordinates system.

3 Calculation of Magnetic Vector Potential

In this section, the general solution of a partial differential equation (PDE) in each subdomain is calculated. Considering the appropriate domain and PDE (Laplace's/Poisson's equation) for each region, the general solution of the PDEs and their corresponding coefficients for each region is estimated by using the separation of variables method take into account the boundary and interface conditions.

3.1 PDE Definition

In Table 1, Laplace's and Poisson's equations for the different regions of the proposed machine are expressed in the pseudo-Cartesian coordinate system. As can be seen, for the stator slot region (region *j*) and the permanent magnet region (region I) the Poisson's equation, and the other regions the Laplace equation is written. The values of M_{rn} and $M_{\theta n}$ for the two conditions of radial and parallel magnetization are given in Table 1.

3.2 BC Definition

Fig. 2 shows Neumann's boundary conditions at the sides (on the *θ-edge*) and the ends (on the *t-edge*) of the represented regions. According to Table 2, Neumann's boundary conditions can be written on the stator slot sides (on the *θ-edge*) and the stator slot top-bottom (on the *t- edge*) of the region *j*. These conditions can also be written for the stator slot opening sides (on the *θ-edge*) of the region *I* and on the dummy slot sides (on the *θ-edge*) and the dummy slot top-bottom (on the *t- edge*) of the region *k*. It is also possible to write Neumann's boundary conditions in the PMs and iron core interface (on the *t- edge*) as presented in Table 2.

3.3 IC Definition

To determine the coefficients in the general solution of Laplace's and Poisson's equations in different regions, it is necessary to write the interface condition equations between two adjacent regions. The number of equations must be equal to the number of unknowns. Therefore, according to Table 3, in the interface conditions of the two adjacent regions, the magnetic vector potential and its first-order differential function are equal.

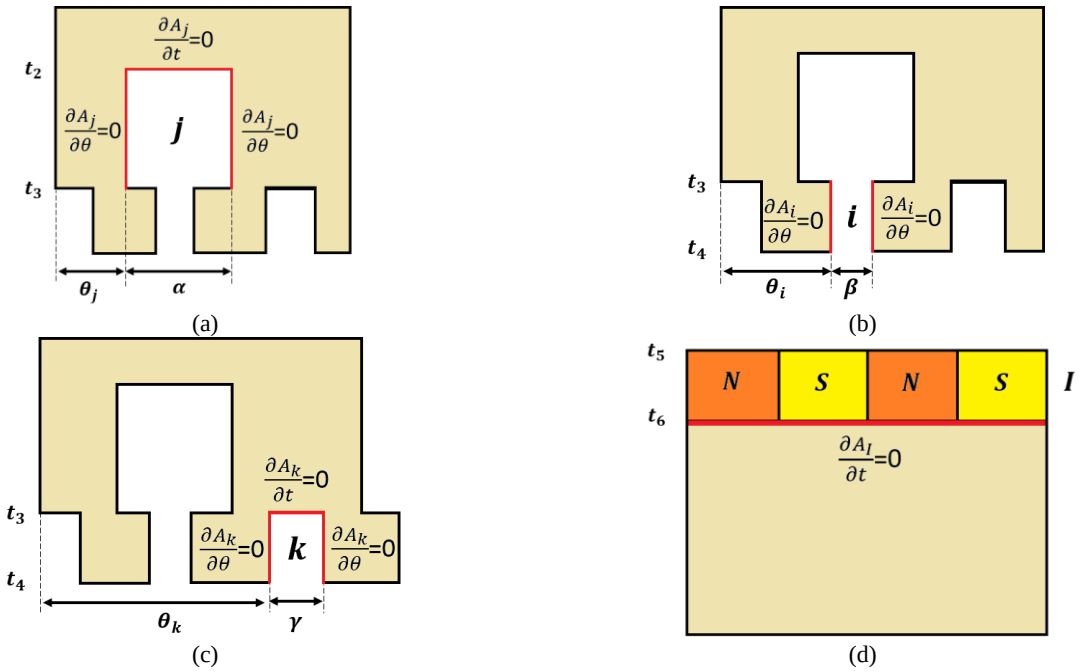

Fig. 2 Neumann's boundary conditions at a) the sides of the stator slot and b) the sides of the stator slot opening, c) the end and sides of the stator dummy slots, d) the rotor yoke.

Table 2 Neumann's boundary conditions at *θ-edges* and *t-edges* of the machine subdomains.

Region	θ-*edge*	Region	*t-edge*
j	$\left.\frac{\partial A_j}{\partial \theta}\right\|_{\theta=\theta_j} = 0$	*j*	$\left.\frac{\partial A_j}{\partial t}\right\|_{t=t_1} = 0$
j	$\left.\frac{\partial A_j}{\partial \theta}\right\|_{\theta=\theta_j+\alpha} = 0$	*k*	$\left.\frac{\partial A_k}{\partial t}\right\|_{t=t_3} = 0$
i	$\left.\frac{\partial A_i}{\partial \theta}\right\|_{\theta=\theta_i} = 0$	*I*	$\left.\frac{\partial A_I}{\partial t}\right\|_{t=t_6} = 0$
i	$\left.\frac{\partial A_i}{\partial \theta}\right\|_{\theta=\theta_i+\beta} = 0$		
k	$\left.\frac{\partial A_k}{\partial \theta}\right\|_{\theta=\theta_k} = 0$		
k	$\left.\frac{\partial A_k}{\partial \theta}\right\|_{\theta=\theta_k+\gamma} = 0$		

3.4 General Solution of PDE

The general solutions of Laplace's and Poisson's differential equations in the regions of the machine are obtained by using the separation of variables method considering Neumann's boundary conditions as given in Table 4. As can be seen, these equations are written in the Cartesian quasi-coordinates system and are in terms of hyperbolic and trigonometric functions, and are written in such a way that the coefficients of the equation can be easily obtained.

Table 3 Interface condition between two adjacent regions in the studied machine.

$\left.\frac{\partial A_j}{\partial t}\right\|_{t=t_2} = f(\theta) = \begin{cases} \left.\frac{\partial A_i}{\partial t}\right\|_{t=t_3} & \text{for } \theta_i \le \theta \le \theta_i + \beta \\ 0 & \text{elsewhere} \end{cases}$	$\mu_0 J_i \sinh(t_1) = \frac{1}{\alpha}\int_{\theta_j}^{\theta_j+\alpha} f(\theta)\,d\theta$ $a_h{}^j = \frac{2}{\alpha}\int_{\theta_j}^{\theta_j+\alpha} f(\theta)\cos\left(\frac{h\pi}{\alpha}(\theta-\theta_j)\right)d\theta$
$Ai(t_3.\theta) = Aj(t_4.\theta)$ for $\theta_i \le \theta \le \theta_i + \beta$	$a_0{}^i + \ln\left(\frac{R_5}{R_6}\right) b_0{}^i = \frac{1}{\beta}\int_{\theta_i}^{\theta_i+\alpha} Aj(t_4.\theta)\,d\theta$ $a_h{}^i = \frac{2}{\beta}\int_{\theta_i}^{\theta_i+\beta} Aj(t_4.\theta)\cos\left(\frac{h\pi}{\beta}(\theta-\theta_i)\right)d\theta$
$Ai(t_4.\theta) = AII(t_5.\theta)$ for $\theta_i \le \theta \le \theta_i + \beta$	$a_0{}^i = \frac{1}{\beta}\int_{\theta_i}^{\theta_i+\beta} AII(t_5.\theta)\,d\theta$ $b_h{}^i = \frac{2}{\beta}\int_{\theta_i}^{\theta_i+\beta} AII(t_5.\theta)\cos\left(\frac{h\pi}{\beta}(\theta-\theta_i)\right)d\theta$
$Ak(t_4.\theta) = AII(t_5.\theta)$ for $\theta_k \le \theta \le \theta_k + \gamma$	$a_0{}^k = \frac{1}{\gamma}\int_{k}^{\theta_k+\gamma} AII(t_5.\theta)\,d\theta$ $a_h{}^k = \frac{2}{\gamma}\int_{k}^{\theta_k+\gamma} AII(t_5.\theta)\cos\left(\frac{h\pi}{\beta}(\theta-\theta_i)\right)d\theta$
$\left.\frac{\partial A_{II}}{\partial t}\right\|_{t=t_5} = g(\theta) = \begin{cases} \left.\frac{\partial A_i}{\partial t}\right\|_{t=t_4} & \theta_i \le \theta \le \theta_i + \beta \\ \left.\frac{\partial A_k}{\partial t}\right\|_{t=t_4} & \theta_k \le \theta \le \theta_k + \gamma \\ 0 & \textit{elsewhere} \end{cases}$	$a_n{}^{II} = \begin{cases} \frac{2}{2\pi}\int_{\theta_i}^{\theta_i+\beta} g(\theta)\cos(n\theta)\,d\theta & \theta_i \le \theta \le \theta_i + \beta \\ \frac{2}{2\pi}\int_{\theta_k}^{\theta_k+\gamma} g(\theta)\cos(n\theta)\,d\theta & \theta_k \le \theta \le \theta_k + \gamma \\ 0 & \text{elsewere} \end{cases}$ $c_n{}^{II} = \begin{cases} \frac{2}{2\pi}\int_{\theta_i}^{\theta_i+\beta} g(\theta)\sin(n\theta)\,d\theta & \theta_i \le \theta \le \theta_i + \beta \\ \frac{2}{2\pi}\int_{\theta_k}^{\theta_k+\gamma} g(\theta)\sin(n\theta)\,d\theta & \theta_k \le \theta \le \theta_k + \gamma \\ 0 & \text{elsewere} \end{cases}$
$\left.\frac{\partial A_{II}}{\partial t}\right\|_{t=t_6} = h(\theta) = \left.\frac{\partial A_I}{\partial t}\right\|_{t=t_7}$ $\theta_k \le \theta \le \theta_k + \gamma$	$b_n{}^{II} = \frac{2}{2\pi}\int_{\theta_k}^{\theta_k+\gamma} h(\theta)\cos(n\theta).d\theta$ $d_n{}^{II} = \frac{2}{2\pi}\int_{\theta_k}^{\theta_k+\gamma} h(\theta)\sin(n\theta).d\theta$
$A_I(t_7.\theta) = A_{II}(t_6.\theta)$	$a_n^I = \frac{2}{2\pi}\int_0^{2\pi} A_{II}(t_6.\theta)\cos(n\theta).d\theta$ $c_n^I = \frac{2}{2\pi}\int_0^{2\pi} A_{II}(t_6.\theta)\sin(n\theta).d\theta$

Table 4 The general solution of Laplace's and Poisson's equations for the proposed PMV machine.

Region Ω	General solution
j, i, k	$A_\Omega(t.\theta)=a_0^\Omega+b_0^\Omega t+f(t)+\sum_{h=1}^{\infty}\left(a_h^\Omega\frac{\varphi}{h\pi}\frac{F\left(\frac{h\pi}{\varphi}(t-t_i)\right)}{G\left(\frac{h\pi}{\varphi}(t_j-t_i)\right)}+b_h^\Omega\frac{\varphi}{h\pi}\frac{F\left(\frac{h\pi}{\varphi}(t-t_i)\right)}{G\left(\frac{h\pi}{\varphi}(t_j-t_i)\right)}\right)\cos\left(\frac{h\pi}{\varphi}(\theta-\varnothing)\right)$
II, I	$A_\Omega(t.\theta)=\sum_{n=1}^{\infty}\left(\frac{1}{n}\frac{F(n(t-t_i))}{G(n(t_j-t_i))}a_n^\Omega+\frac{1}{n}\frac{F(n(t-t_j))}{G(n(t_i-t_j))}b_n^\Omega+g(t)\right)\cos(n\theta)$ $+\sum_{n=1}^{\infty}\left(\frac{1}{n}\frac{F(n(t-t_i))}{G(n(t_j-t_i))}c_n^\Omega+\frac{1}{n}\frac{F(n(t-t_j))}{G(n(t_i-t_j))}d_n^\Omega+g(t)\right)\sin(n\theta)$

where $f(t)=-\frac{1}{2}\mu_0 J_i\left(e^{-t_1}t+\frac{1}{2}e^{-2t+t_1}\right)$, $\varphi=\alpha$, $\phi=\theta_j$, $b_0^\Omega=b_h^\Omega$, $t_i=t_1$, and $t_j=t_2$, F=cosh, G=sinh at j region, $f(t)=0$, $\varphi=\beta$, $\phi=\theta_i$, $t_i=t_3$, and $t_j=t_4$, F=sinh, G=sinh at I region, $f(t)=0$, $\varphi=\gamma$, $\phi=\theta_k$, $b_0^\Omega=b_h^\Omega=0$, $t_i=t_3$, and $t_j=t_4$, F=cosh, G=sinh at k region, F=cosh, G=sinh, $t_i=t_6$, and $t_j=t_5$, and F=cosh, G=cosh, $t_i=t_8$, and $t_j=t_7$, $g(t)=X_n(t)\cos\left(\frac{n\pi\alpha_p}{2\alpha_r}\right)$,

$$X_n(t)=\left(1+\frac{1}{n}e^{(n+1)t}\right)f_n(t)-\frac{\cosh(n(t-t_8))}{\cosh(n(t_7-t_8))}\left(1+\frac{1}{n}e^{(n+1)t_7}\right)f_n(t_7) \tag{6}$$

$$f_n(t)=\begin{cases}\mu_0\dfrac{npM_{rn}+M_{\theta n}}{1-np^2}R_1e^{-t} & \text{if } np\neq 1\\ -\mu_0\dfrac{M_{rn}+M_{\theta n}}{2}R_1e^{-t}\ln\left(R_1e^{-t}\right) & \text{if } np=1\end{cases} \tag{7}$$

Table 5 Performance calculation of a 3-phase brushless permanent magnet machine.

$T_e=\frac{L_s}{\mu_0}\int_0^{2\pi}BI_r(t_e.\theta).BI_\theta(t_e.\theta)\,d\theta \qquad t_e=\ln\left(\frac{R_2}{R_e}\right), \quad R_e=(R_2+R_3)/2$ (8)
$\begin{bmatrix}\psi_a\\ \psi_b\\ \psi_c\end{bmatrix}=N_cC^T\begin{bmatrix}\varphi_1 & \varphi_2 & \varphi_3 & \dots & \varphi_{Q_2}\end{bmatrix}$ (9)
$\varphi_i=-\frac{L_sR_4^2}{k_fS}\int_0^{\beta}\int_0^{t_8}A_{mi}(t.\theta).e^{-2t}dtd\theta$ (10)
$\begin{bmatrix}\psi_a\\ \psi_b\\ \psi_c\end{bmatrix}=\begin{bmatrix}\psi1_a\\ \psi1_b\\ \psi1_c\end{bmatrix}+\begin{bmatrix}\psi2_a\\ \psi2_b\\ \psi2_c\end{bmatrix} \qquad \begin{bmatrix}\psi1_a\\ \psi1_b\\ \psi1_c\end{bmatrix}=\frac{N_c}{2}C_1^T\begin{bmatrix}\varphi_{11} & \varphi_{12} & \varphi_{13} & \dots & \varphi_{1Q_2}\end{bmatrix}, \begin{bmatrix}\psi2_a\\ \psi2_b\\ \psi2_c\end{bmatrix}=\frac{N_c}{2}C_2^T\begin{bmatrix}\varphi_{21} & \varphi_{22} & \varphi_{23} & \dots & \varphi_{2Q_2}\end{bmatrix}$ (11)
$\varphi_{1i}=-\frac{2L_sR_4^2}{k_fS}\int_0^{\frac{\beta}{2}}\int_0^{t_8}A_{mi}(t.\theta).e^{-2t}dtd\theta$ (12)
$\varphi_{2i}=-\frac{2L_sR_4^2}{k_fS}\int_{\frac{\beta}{2}}^{\beta}\int_0^{t_8}A_{mi}(t.\theta).e^{-2t}dtd\theta$ (13)
$E_a=\omega\frac{d\psi_a}{d\theta_r}$ (14)
$L_a=\frac{\psi_a}{I_A}$ (15)
$M_{AB}=\frac{N\varphi_{AB}}{I_B}$ (16)

Table 6 Parameter definition.

Parameter	Description
T_e	Electromagnetic torque
L_s	Axial length of the motor
R_e	Effective radius
N_c	Number of conductors per slot
C	A matrix connection between the stator slots and phase connections
φ	The slot flux
k_f	The stator fill factor
S	The area of the stator slot
Ω	The rotor angular speed
ψ_a	flux linkage per phase A
I_A	The peak current in phase A
E_a	The phase A back-emf
L_a	Self-inductance of phase A
M_{AB}	Mutual inductance of phase A and phase B
N	The number of phase turns
φ_{AB}	Magnetic flux in phases A and B
I_B	The peak current in phase B

Table 7 Geometrical parameters and their corresponding values for the investigated machine.

Parameter	Value [mm]	Parameter	Value [degree]
R_1	180	θ_i	2.5
R_2	248	θ_j	7
R_3	250	θ_k	10
R_4	252	β	2.5
R_5	367	α	2.5
R_6	450	γ	5

Table 8 Parameters of the investigated machine.

Parameter	Description	Value
p	Number of rotor's pole pairs	12
Q_{ds}	Number of stator's dummy slots	36
Q_s	Number of stator's slots	36
B_r	Residual flux density of PM	1.2 [T]
L_s	Axial length of machine	300 [mm]
n	Rotational speed	150 [rpm]
P	Rated power	14 [kW]

Fig. 3 Stator laminations with dummy slots.

Fig. 4 The fabricated surface mounted rotor.

3.5 Machine Performance

In this section, the performance characteristics of a three-phase brushless permanent magnet motor are calculated. As given in Table 5, the electromagnetic torque, the flux linkages, back-emf, self-inductance, and mutual inductance can be calculated by (8) to (16), respectively.

4 Model Evaluation

In this section, we first describe the steps for the fabrication of a BLDC motor and performing open circuit and load tests. Then numerical modeling and analysis are presented in the Maxwell software environment. In the end, the analytical, experimental, and numerical results of the magnetic flux, electromagnetic torque, cogging torque, back-electromotive force, self-inductance, and mutual inductance are compared.

4.1 Motor Fabrication and Experimental Test

To evaluate the accuracy of the proposed analytical model, a 14kW, 150rpm, 24 poles-36 slots, three-phase two-layer winding BLDC motor were designed and fabricated. The motor's rotor, equipped with radially magnetized N-42 NdFeB permanent magnets. Dummy slots were punched in stator teeth to reduce the pulsating.

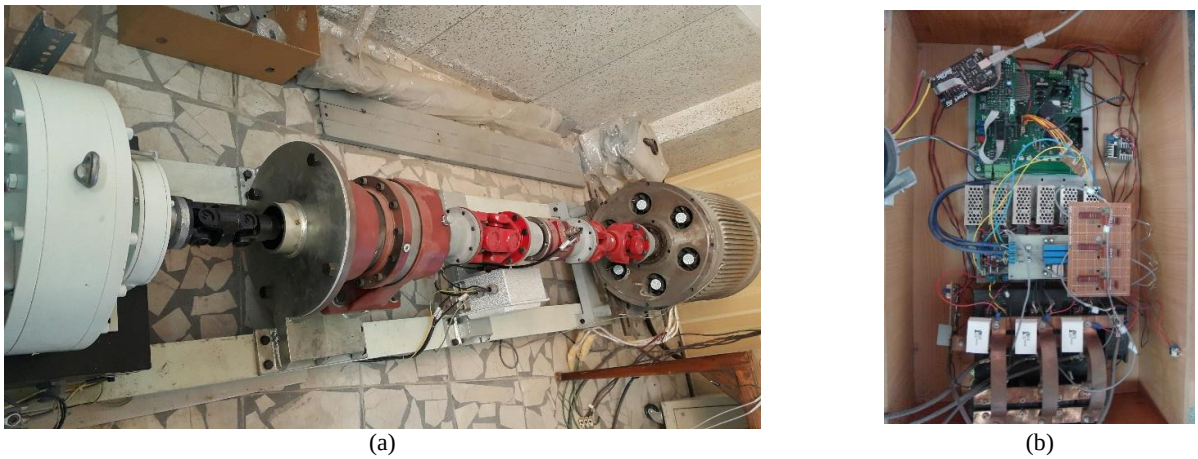

(a) (b)

Fig. 5 Test setup; a) the fabricated BLDC permanent magnet motor during testing on a dynamometer and b) the fabricated drive.

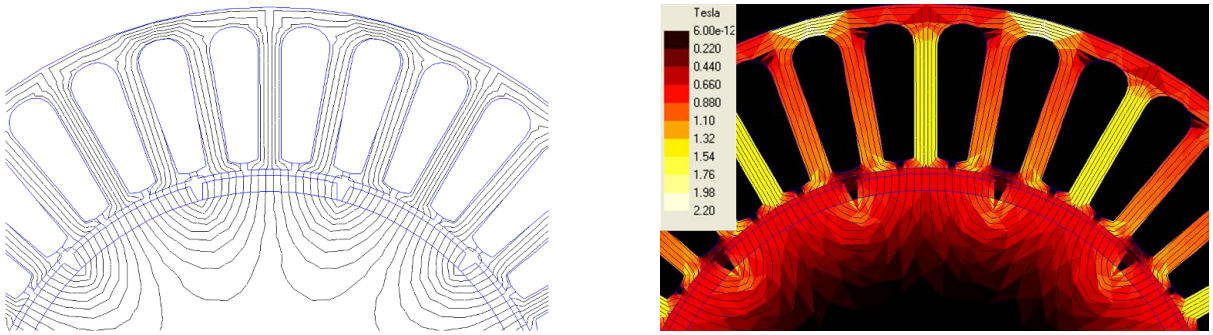

(a) (b)

Fig. 6 Two-dimensional analysis of the BLDC motor without dummy slots. a) magnetic flux line distribution and b) magnetic flux density distribution.

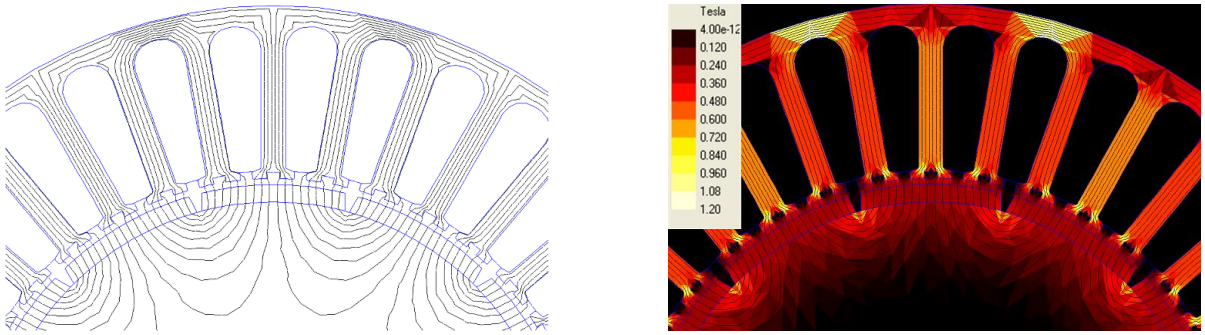

(a) (b)

Fig. 7 Two-dimensional analysis of the BLDC motor with dummy slots. a) magnetic flux line distribution and b) magnetic flux density distribution.

The rotor's and stator's cores were punched using a press dies, and after being pressurized by a hydraulic press, they were joined by TIG welding.

Table 6 lists the brushless motor parameters, symbols, and their corresponding values. Fig. 3 shows the laminated core of the stator, in which dummy slots are punched to reduce the cogging torque. Fig. 4 shows the rotor of the investigated machine. Fig. 5(a) shows how the motor is connected to the dynamometer. The motor drive is also shown in Fig. 5(b). Experimental tests have been performed to measure the motor performance in open circuit/on-load conditions. An open circuit test is performed to measure cogging torque. To determine the motor's electromagnetic torque/magneto-motive force waveforms, the motor performance in the full-load condition is examined.

4.2 FEA Simulation

The two-dimensional analysis of the studied BLDC motor with/without dummy slot was performed in the Maxwell software and the distribution of magnetic flux lines and their flux density were shown in Figs. 6 and 7, respectively.

4.3 Analytical, Experimental and Numerical Comparison

To investigate the effect of dummy slots on the

magnetic flux density distribution in the air-gap region of the studied motor in open circuit and under full-load conditions, the results of the proposed analytical model are compared with the results of numerical simulations and experimental tests. Fig. 8(a) shows the air-gap magnetic flux density waveforms in the BLDC motor without any dummy slot in open circuit conditions. Fig. 8(b) shows the air-gap magnetic flux density distribution in the BLDC motor with dummy slots in open circuit conditions. Fig. 9 compares the cogging torque waveforms of the investigated machine with dummy slots in open circuit conditions resulting from both experimental and analytical methods. In full-load condition, the electromagnetic torque waveforms, the back-emf waveforms, the phase-inductance, and the mutual inductance of motor are calculated by analytical method and compared with the results of experimental tests as shown in Figs. 10-13, respectively.

5 Conclusion

In this paper, an accurate two-dimensional analytical method for calculating the magnetic vector potential in a brushless permanent magnet machine is provided to take into account the effect of stator slots, dummy slots, winding combination, and magnetization direction. To facilitate modeling, by applying the variable change and converting the polar coordinates to the pseudo-Cartesian

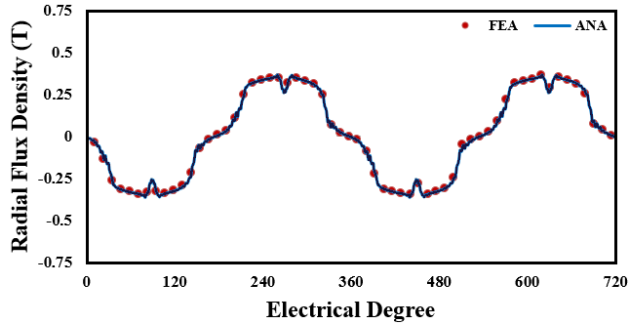

(a)

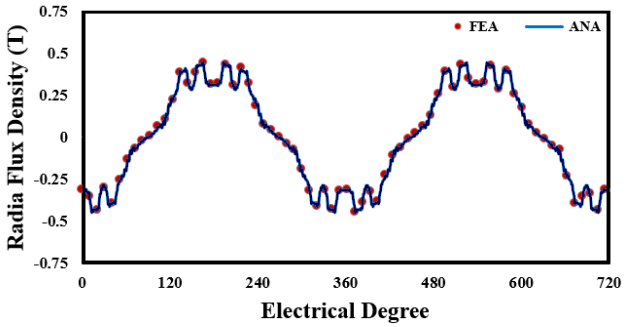

(b)

Fig. 8 An analytical and numerical comparison of radial flux density waveforms in the middle of air-gap in open circuit condition for the investigated machine a) without dummy slots and b) with dummy slots.

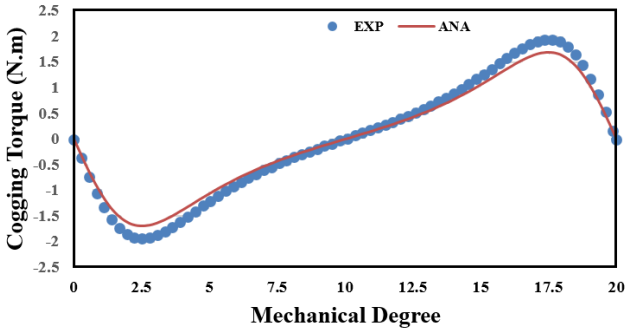

Fig. 9 An analytical and experimental comparison of the cogging torque waveforms in the investigated motor with dummy slots in no-load condition.

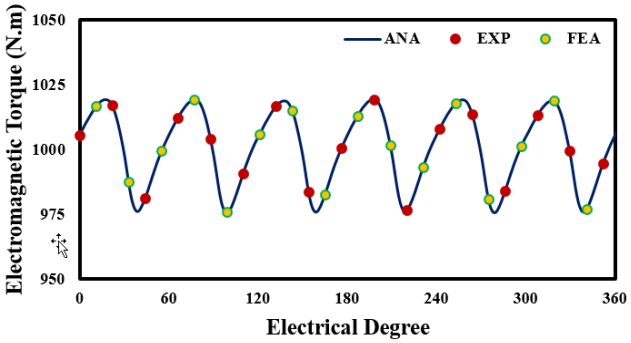

Fig. 10 An analytical, numerical, and experimental comparison of the electromagnetic torque waveforms in the investigated motor with dummy slots in full-load condition.

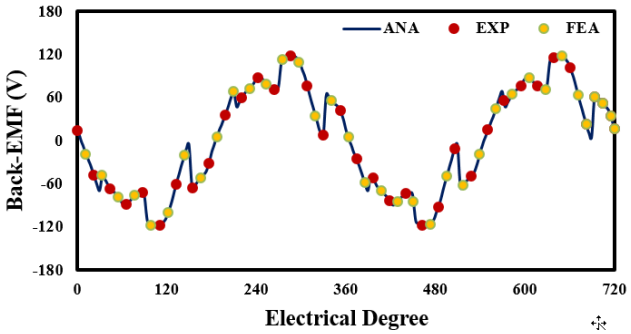

Fig. 11 An analytical, numerical, and experimental comparison of the Back-EMF waveforms in the investigated motor with dummy slots in full-load condition

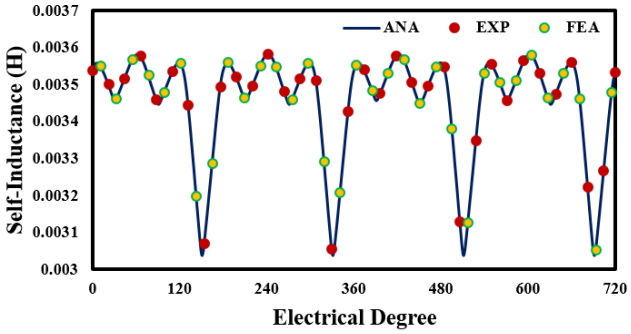

Fig. 12 An analytical, numerical, and experimental comparison of the self-inductance waveforms in the investigated motor with dummy slots in full-load condition.

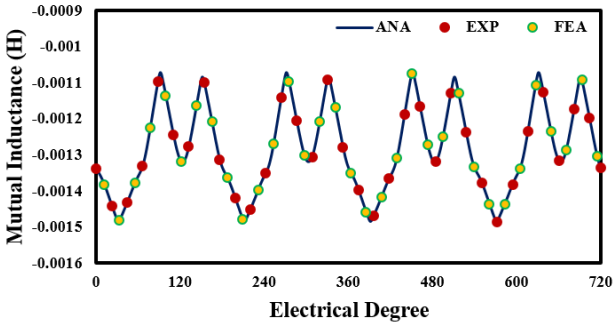

Fig. 13 An analytical, numerical, and experimental comparison of the mutual inductance waveforms in the investigated motor with dummy slots in full-load condition.

coordinates, by applying the boundary conditions and the corresponding interface conditions of each region, the magnetic vector potential expressions for those regions were formulated. To validate the proposed analytical model, a 24-pole, 36-slot, 150 rpm, 14-kW permanent magnet motor was designed, fabricated and its characteristics were extracted. A two-dimensional model was also created in the finite element analysis software environment, and the motor performance waveforms in open circuit and under load conditions were compared. By comparing the analytical, numerical, and experimental results, it can be seen that the proposed model accurately estimates the performance of a brushless permanent magnet motor.

Intellectual Property

The authors confirm that they have given due consideration to the protection of intellectual property associated with this work and that there are no impediments to publication, including the timing of publication, with respect to intellectual property.

Funding

No funding was received for this work.

CRediT Authorship Contribution Statement

A. Jabbari: Conceptualization, Methodology, Software, Formal analysis, Writing - Original draft.

Declaration of Competing Interest

The authors hereby confirm that the submitted manuscript is an original work and has not been published so far, is not under consideration for publication by any other journal and will not be submitted to any other journal until the decision will be made by this journal. All authors have approved the manuscript and agree with its submission to "Iranian Journal of Electrical and Electronic Engineering".

References

[1] M. Lukaniszyn, M. Jagiela, and R. Wrobel, "Optimization of permanent magnet shape for minimum cogging torque using a genetic algorithm," *IEEE Transactions on Magnetics*, Vol. 40, No. 2, pp. 1228–1231, 2004.

[2] D. C. Hanselman, "Effect of skew, pole count and slot count on brushless motor radial force, cogging torque and back EMF," *IEE Proceedings-Electric Power Applications*, Vol. 144, No. 5, pp. 325–330, 1997.

[3] R. Lateb, N. Takorabet, and F. Meibody-Tabar, "Effect of magnet segmentation on the cogging torque in surface-mounted permanent-magnet motors," *IEEE Transactions on Magnetics*, Vol. 42, No. 3, pp. 442–445, 2006.

[4] B. Ackermann, R. Sottek, J. H. H. Janssen, and R. I. Van Steen, "New technique for reducing cogging torque in a class of brushless DC motors," *IEE Proceedings B (Electric Power Applications)*, Vol. 139, No. 4, pp. 315–320, 1992.

[5] T. Ishikawa and G. R. Slemon, "A method of reducing ripple torque in permanent magnet motors without skewing," *IEEE Transactions on Magnetics*, Vol. 29, No. 2, pp.2028–2031, 1993.

[6] A. Keyhani, C. Studer, T. Sebastian, and S. K. Murth, "Study of cogging torque in permanent magnet motors," *Electric Machines and Power Systems*, Vol. 27, No. 7, pp. 665–678, Jul. 1999.

[7] T. Li, and G. Slemon, "Reduction of cogging torque in permanent magnet motors," *IEEE Transactions on Magnetics*, Vol. 24, No. 6, pp. 2901–2903, 1988.

[8] C. C. Hwang, S. B. John, and S. S. Wu, "Reduction of cogging torque in spindle motors," *IEEE Transactions on Magnetics*, Vol. 34, No. 2, pp. 468–470, 1998.

[9] Z. Q. Zhu and D. Howe, "Instantaneous magnetic-field distribution in brushless permanent-magnet dc motor, part III: Effect of slotting," *IEEE Transactions on Magnetics*, Vol. 29, No. 1, pp. 143–151, Jan. 1993.

[10] M. Markovic, M. Jufer, and Y. Perriard, "Reducing the cogging torque in brushless dc motors by using conformal mappings," *IEEE Transactions on Magnetics*, Vol. 40, No. 2, pp. 451–455, Mar. 2004.

[11] D. Zarko, D. Ban, and T. A. Lipo, "Analytical calculation of magnetic field distribution in the slotted air gap of a surface permanent-magnet motor using complex relative air-gap permeance," *IEEE Transactions on Magnetics*, Vol. 42, No. 7, pp. 1828–1837, Jul. 2006.

[12] K. Boughrara, D. Zarko, R. Ibtiouen, O. Touhami, and A. Rezzoug, "Magnetic field analysis of inset and surface-mounted permanent-magnet synchronous motor using Schwarz-Christoffel transformation," *IEEE Transactions on Magnetics*, Vol. 45, No. 8, pp. 3166–3168, Aug. 2009.

[13] E. Ilhan, B. L. J. Gysen, J. J. H. Paulides and E. A. Lomonova "Analytical hybrid model for flux switching permanent magnet machines," *IEEE Transactions on Magnetics*, Vol. 46, No. 6, pp. 1762–1765, Jun. 2010.

[14] Y. Tang, T. E. Motoasca, J. J. H. Paulides, and E. A. Lomonova, "Analytical modeling of flux-switching machines using variable global reluctance networks," in *XXth International Conference on Electrical Machines (ICEM)*, pp. 2792–2798, Sep. 2012.

[15] W. Hua, G. Zhang, M. Cheng and J. Dong "Electromagnetic performance analysis of hybrid-excited flux-switching machines by a nonlinear magnetic network model," *IEEE Transactions on Magnetics*, Vol. 47, No. 10, pp. 3216–3219, Oct. 2011.

[16] A. Jabbari, "2D Analytical Modeling of Magnetic Vector Potential in Surface Mounted and Surface Inset Permanent Magnet Machines," *Iranian Journal of Electrical and Electronic Engineering*, Vol. 13, No. 4, pp. 362–373, 2017.

[17] A. Jabbari, "Exact analytical modeling of magnetic vector potential in surface inset permanent magnet DC machines considering magnet segmentation," *Journal of Electrical Engineering*, Vol. 69, No. 1, pp. 39–45, 2018.

[18] A. Jabbari, "Analytical modeling of magnetic field distribution in inner rotor brushless magnet segmented surface inset permanent magnet machines," *Iranian Journal of Electrical and Electronic Engineering*, Vol. 14, No. 3, pp. 259–269, 2018.

[19] A. Jabbari, "Analytical modeling of magnetic field distribution in multiphase H-type stator core permanent magnet flux switching machines," *Iranian Journal of Science and Technology, Transactions on Electrical Engineering*, Vol. 43, No. 1, pp. 389–401, Jul. 2019.

[20] A. Jabbari, "An analytical expression for magnet shape optimization in surface-mounted permanent magnet machines," *Mathematical and Computational. Applications*, Vol. 23, No. 4, p. 57, 2018.

[21] A. Jabbari, "An analytical study on iron pole shape optimization in high-speed interior permanent magnet machines," *Iranian Journal of Science and Technology, Transactions on Electrical Engineering*, Vol. 44, No. 1, pp.169–174, 2020.

[22] A. Jabbari and F. Dubas, "A new subdomain method for performances computation in interior permanent-magnet (IPM) machines," *Iranian Journal of Electrical and Electronic Engineering*, Vol. 16, No. 1, pp. 26–38, Mar. 2020.

[23] A. Jabbari "An analytical, numerical and experimental study on performance characteristics in a novel vernier permanent magnet machine," *Electrical Engineering*, Vol. 102, No. 4, pp. 2369–2379, 2020.

[24] B. Gaussens, E. Hoang, O. de la Barriere, J. Saint-Michel and M. Gabsi "Analytical approach for air-gap modeling of field-excited flux- switching machine: No-load operation," *IEEE Transactions on Magnetics*, Vol. 48, No. 9, pp. 2505–2517, 2012.

[25] B. Gaussens, E. Hoang, O. de la Barriere, J. Saint-Michel, P. Manfe, M. Lecrivain, and M. Gabsi "Analytical armature reaction field prediction in field-excited flux-switching machines using an exact relative permeance function," *IEEE Transactions on Magnetics*, Vol. 49, No. 1, pp.628–641, 2013.

A. Jabbari was born in Shazand, Iran, in 1980. He received the B.Sc. degree from Iran University of Science and Technology in 2002 and his M.Sc. and Ph.D. degrees both in Mechanical Engineering from Mazandaran University in 2004 and 2009, respectively, with a focus on the design and optimization of brushless DC permanent magnet machines for direct drive applications. He is currently an Associate Professor with the Department of Mechanical Engineering, Arak University, Arak, Iran. Since 2014, he has been the head of the "Gearless Wind Turbine Project" team. His research interests are gearless wind turbine design, analytical modeling, PM machines, subdomain technique, friction stir welding, and metal forming.